Journal of Structural Geology 32 (2010) 1363–1374

Contents lists available at ScienceDirect

Journal of Structural Geology

journal homepage: www.elsevier.com/locate/jsg

Integrated fracture prediction using sequence stratigraphy within a carbonate fault damage zone, Texas, USA

Christopher K. Zahm*, Laura C. Zahm, Jerome A. Bellian

Bureau of Economic Geology, The University of Texas at Austin, Jackson School of Geosciences, University Station, Box X, Austin, TX 78712, United States

ARTICLE INFO

Article history:
Received 21 February 2008
Received in revised form 18 May 2009
Accepted 20 May 2009
Available online 6 June 2009

Keywords:
Sequence stratigraphy
Fractures
Carbonate
TST
HST
Fault damage zone

ABSTRACT

Fracture deformation intensity is heterogeneous as a result of the interplay between the stratigraphic architecture and the degree of faulting. Prediction of the distribution of fractures requires careful consideration of the sequence stratigraphic framework in concert with the structural deformation process. Deformation intensity was found to vary by facies that were divided into distinct mechanical units and characterized within a sequence stratigraphic framework. Deformation was found to be more intensely developed within the transgressive systems tract (TST) versus the highstand systems tract (HST). In the HST, facies observed in the outcrop from this study had less mud, thicker cycles, and higher unconfined strength (average of 57 MPa for non-argillaceous facies). In contrast, the TST cycle sets have a higher argillaceous component and cycles are thinner. The facies have a higher mud content and lower unconfined strength (average of 49 MPa for non-argillaceous facies). The reduction in rock strength is compounded by thinner beds and increased frequency of argillaceous wackestone beds. The TST facies also affect the geometry of secondary faults, creating asperities along the fault plane that cause further deformation. Overall, the integration of facies, rock strength and mud content within a sequence stratigraphic framework provides an improved methodology for prediction of deformation within a carbonate fault damage zone.

1. Introduction

Fractures in the subsurface, as with any geologic phenomena, must be correlated to mappable surfaces such as stratigraphic horizons or faults if three-dimensional characterization is to be accomplished in the subsurface. The stratigraphic architecture is a primary controlling factor on fracture development as it dictates the distribution and variability of sedimentary facies which influences the style, intensity, and location of fractures. Furthermore, understanding the impact that fractures may exert on fluid flow in the subsurface requires the incorporation of fractures within an integrated model that includes petrophysical properties of the matrix and fractures—specifically porosity, permeability, and water saturation. The stratigraphic framework represents the foundation for construction of models that incorporate rock properties. A logical progression for characterizing fracture development is to relate fractures to the existing stratigraphic derived rock property model. Structural deformation such as faulting also has a significant impact on fracture development, and ultimately on the flow behavior in the subsurface (Caine et al., 1996). It is important to consider the influence of both stratigraphy and structural deformation in concert, rather than separately, if predictability of fracture distribution is to be maximized.

The relation between fractures and stratigraphy—namely mechanical stratigraphy—has been demonstrated by correlating bed thickness with fracture intensity (McQuillan, 1973; Ladeira and Price, 1981; Huang and Angelier, 1989; Narr and Suppe, 1991; Gross, 1993; Wu and Pollard, 1995; Bai and Pollard, 2000; Lorenz et al., 2002; Renshaw et al., 2003). Alternatively, fracture intensity has been correlated to petrologic rock properties such as strength or ductility (Cook and Erdogan, 1972; Huang and Zhang, 1995; Biot et al., 1983; Corbett et al., 1987; Thiercelin et al., 1987; Friedman et al., 1994; Rijken and Cooke, 2001; Underwood et al., 2003). Other researchers have focused on the relations between fractures within stratified units and fault zones (Cox and Scholz, 1988; Treagus, 1988; Childs et al., 1996; Walsh et al., 1999, 2003; Wilkins and Gross, 2001; Ferrill and Morris, 2003; Schopfer et al., 2007).

Many of the aforementioned studies have been performed in siliclastic rocks and have had relatively good success correlating fracture intensity to bedding thickness, while correlation to rock strength have been less straightforward. Examples of fracture characterization in carbonates are less common, especially with

* Corresponding author. Tel.: +1 512 471 3159; fax: +1 512 471 0140.
E-mail address: chris.zahm@beg.utexas.edu (C.K. Zahm).

0191-8141/$ – see front matter © 2009 Elsevier Ltd. All rights reserved.
doi:10.1016/j.jsg.2009.05.012

respect to correlating fracture development to sedimentary facies. Exceptions include Friedman et al. (1994) and Corbett et al. (1987), who found a correlation between increased fracture intensity and bed thickness, especially if mineralogy of the chalk is considered (specifically smectite presence) in the Upper Cretaceous Austin Chalk Formation. Gross (1993), and Gross et al. (1995), looked at fracture terminations and opening-mode fracture development in the diatomaceous, chert-rich Miocene Monterrey Formation. Gross and Eyal (2007) studied through going fractures in chalk carbonates of Israel. In both the Monterrey and chalks of Israel, detailed analysis of facies or rock properties were not performed. Underwood et al. (2003) studied Silurian dolomites without achieving relevant correlation between facies, rock strength, and fracture intensity largely due to complication of pervasive dolomitization that homogenized rock strength. Ferrill and Morris (2008) documented the controls of mechanical stratigraphy on the variable response of the strata to deformation, which are controlled by the relative amounts of competent versus incompetent strata.

Other researchers have focused on the relations between fractures within stratified units and fault zones (Cox and Scholz, 1988; Treagus, 1988; Childs et al., 1996; Walsh et al., 1999, 2003; Wilkins and Gross, 2001; Ferrill and Morris, 2003; Schopfer et al., 2007). It is clear from these studies that the faulting process is the primary deformation mechanism, but the heterogeneity observed in fracture intensity within each zone is heavily controlled by the strata, specifically the vertical stacking of facies. The present contribution builds upon work done by Ferrill and Morris (2008), which demonstrated the relationship between fracture development and the relative proportion of incompetent to competent strata within the vertical section. This study further focuses the discussion within a sequence stratigraphic framework which is more predictive than the purely lithofacies derived context they utilize. For instance, an examination of a well log or core will give a precise measurement of the incompetent to competent rock strength ratio for an individual sample location. However, describing the facies within the context of sequence stratigraphic framework allows prediction and distribution of the relative facies proportions in 3D, enabling facies and fracture prediction within the interwell region of subsurface reservoirs.

This study documents brittle deformation intensity, primarily opening-mode and shear fractures, using sequence stratigraphy and extensional faulting as an integrated methodology for a distributed zone of significant fracture develop. We propose that understanding of the sequence stratigraphic framework provides an improved predictability for fracture development within fault zones. Furthermore, we contend that characterization of carbonate fault damage zones in absence of a stratigraphic framework will always give a misleading prediction of fracture distribution and, ultimately, permeability within the fractured subsurface.

2. Regional setting

Extensional faults associated with the Balcones Fault Zone of central Texas occur within primarily Aptian–Albian age carbonates, often the youngest rock exposed, developed during the Late Oligocene to Miocene (Weeks, 1945). These large scale extensional faults are parallel to the paleo-hinge line, set up by the transition between the Comanche Shelf and the Gulf of Mexico Basin. Regional faults exhibit high fracture intensity, which become areas where significant groundwater recharge occurs to the Edwards aquifer (Collins and Hovorka, 1997). Faults have variable amounts of offset throughout the Balcones Fault Zone, creating a hierarchy of fault size based on offset (Fig. 1). Regional scale faults have offsets greater than 30 m, with a maximum up to 259 m (Hill, 1890; Sellards, 1919; Hovorka et al., 1998; Collins, 2000). In standard seismic acquisition and processing, faults of this scale are resolvable. Local faults have offsets between 5 and 30 m, which have been mapped throughout most of the San Antonio area by Collins (2000). Faults of this scale are sub-seismic resolution and represent a significant characterization challenge in subsurface reservoirs. At the outcrop exposure scale, numerous secondary faults (offsets between 10 cm and 5 m) exist which are only detectable by advanced geophysical characterization techniques and direct sampling such as rock coring or downhole logging tools. This study characterizes a local fault with numerous secondary faults in an area north of Bulverde, Texas (Fig. 1, Latitude: 29.775982°, Longitude: −98.424807°).

The exposed section is within the Albian age, Lower Glen Rose Formation. Depositionally, the facies are comprised of predominantly shallow subtidal carbonates of the Albian 6 Composite Sequence, which have been correlated regionally by Loucks and Kerans (2003). The outcrop is located approximately 25 km landward of the Cretaceous Stuart City Reef Margin (Goldhammer, 1999). This reef margin existed as a major break between the platform interior and deeper basinal sediments throughout the Aptian and Albian section. Many of the larger scale extensional faults parallel this stratigraphic margin. The facies succession in this study represents a typical greenhouse succession (Read, 1995), with minor base level changes during deposition that resulted in laterally continuous, vertically stacked cycles of subtidal facies. The depositional succession described is subdivided into six key facies divisions. The most distinct and critical to the mechanical stratigraphy is the most distal facies which consists of an argillaceous wackestone. The presence of mechanical units causes a distributed and variable fracture development that, in the context of a stratigraphic and structural framework, can be used for subsurface applications.

3. Characterization techniques

Panoramic photos were used to interpret the key horizons, local faults (here called the Main Fault), secondary faults, shear fractures, and opening-mode joints (Fig. 2). Nine distinct argillaceous wackestone beds formed recessive notches in the outcrop, and mark stratigraphic cycle bases. These recessively weathered facies and are important fracture termination surfaces. Faults and most fractures in the photos are not interpreted parallel to strike, causing the fractures to have apparent lower dip angle.

The interpretation of fault and fracture orientations along with the recessive argillaceous units was improved by using a ground-based lidar survey. The lidar survey provided a 1–4 cm point spaced location along the outcrop wall. For the excavation and road cut exposures, over 39 million points were surveyed and processed according to methods described in Janson et al. (2007). The lidar survey enabled the measurement of strike and dip for most fractures in the outcrop including faults, shear fractures and opening-mode joints. Significant advantages of lidar surveys measurements is that direct human access is not required to map features exposed on the outcrop; orientation measurements are possible on any face of the outcrop as long as they are within the line of sight of the lidar camera. Fracture and fault planes can be difficult to observe in outcrop especially with variable sunlight angles. Lidar overrides this bias and provides a value of intensity of reflectance that is a quantifiable attribute. Furthermore, interpretation and visualization software can be used to manipulate shading angle, intensity and additional attributes such as surface curvature, which can be used to illuminate different fracture sets and orientations. However, there are limitations to lidar surveying. Fracture orientation is more difficult to determine if the fractures are sub-parallel to the outcrop face, especially with automated techniques. In addition, it is nearly impossible to detect veins or cement-filled joints if they are below the resolution of the lidar survey and remotely sensed fractures that

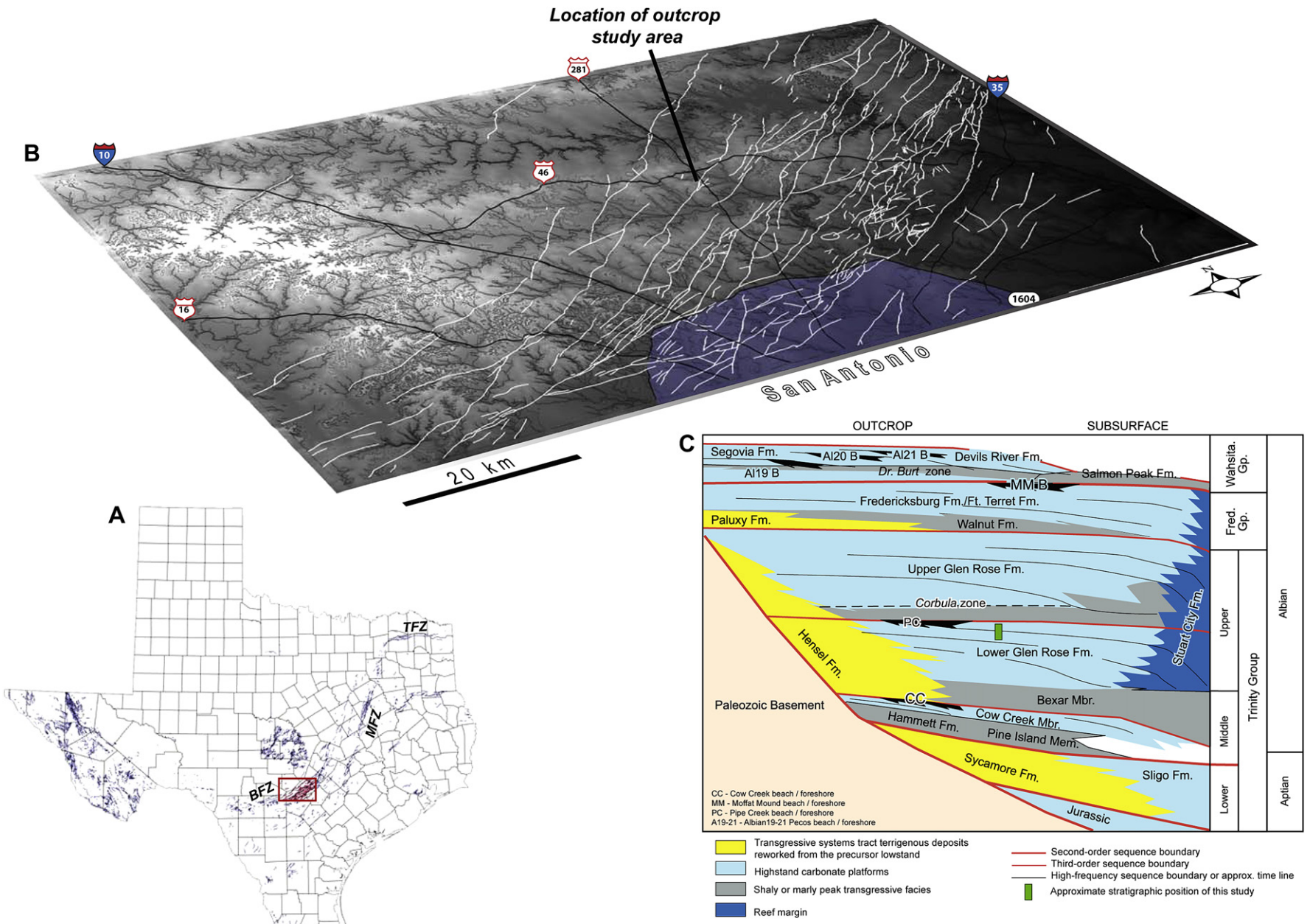

Fig. 1. Location and stratigraphic framework of the study area. (A) Mapped faults in the State of Texas, including the Balcones (BFZ), Talco (TFZ) and Mexia fault zones (MFZ). The inset box represents the expanded area shown in (B); (B) oblique digital elevation model with mapped faults from Collins (2000) illustrating the length and frequency of faults in the study area. Most faults shown here dip between 70 and 85°; and (C) stratigraphic framework of the Aptian–Albian cycles of Texas (modified from Kerans and Loucks, 2002).

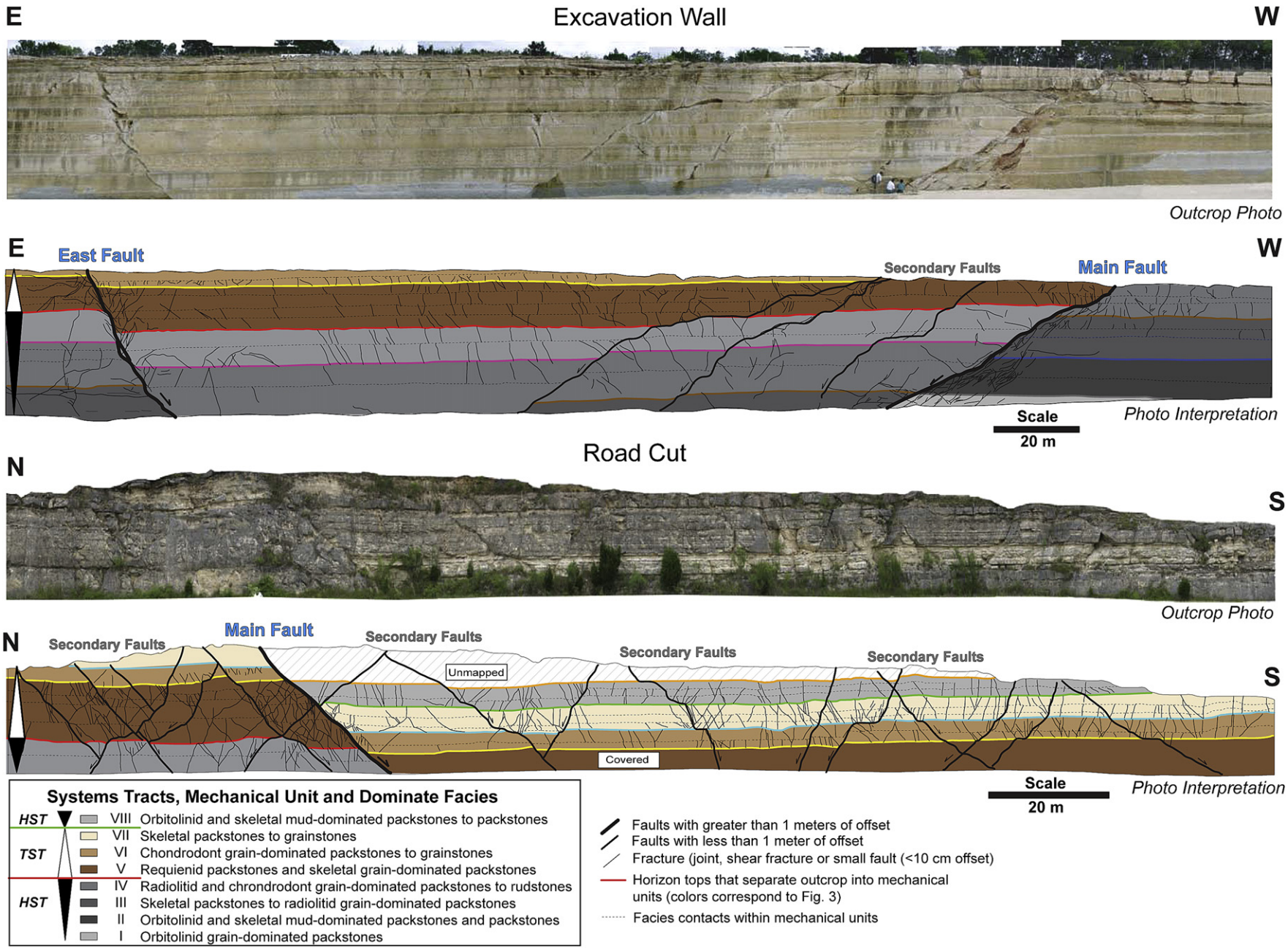

Fig. 2. Photopanoramic tracing of horizons, faults, and fractures of the excavation wall and road cut exposures. Mechanical units are shaded on each interpretation and match the measured section of Fig. 3.

cannot be directly observed are difficult to characterize as opening-mode joints, veins or shear fractures.

Critical to understanding the fracture behavior with respect to stratigraphy, facies were mapped and described through five measured sections to develop a composite measured section for the entire study area (Fig. 3). The measured sections were geometrically corrected to match the lidar survey, enabling precise thickness information for each facies. The composite measured section from this outcrop has been described using a modified Dunham classification scheme (Dunham, 1962; Lucia, 1995). Core plugs were sampled in every facies and tested in a laboratory to determine total porosity and density. In addition, rock strength was estimated by using a rebound hammer, sometimes referred to as a Schmidt hammer. Tests were conducted in accordance with methods described in Poole and Farmer (1980) and ISTM guidelines for measurement collection. The rebound values were converted to unconfined strength (UCS) values using the methods of Deere and Miller (1966) for sedimentary rocks, in order to make comparisons with rocks of similar strength. Petrographic thin sections were prepared for each core plug to examine the pore structure, grain types, and to enhance facies descriptions from outcrop. Finally, a scintillometer survey was conducted along all five measured

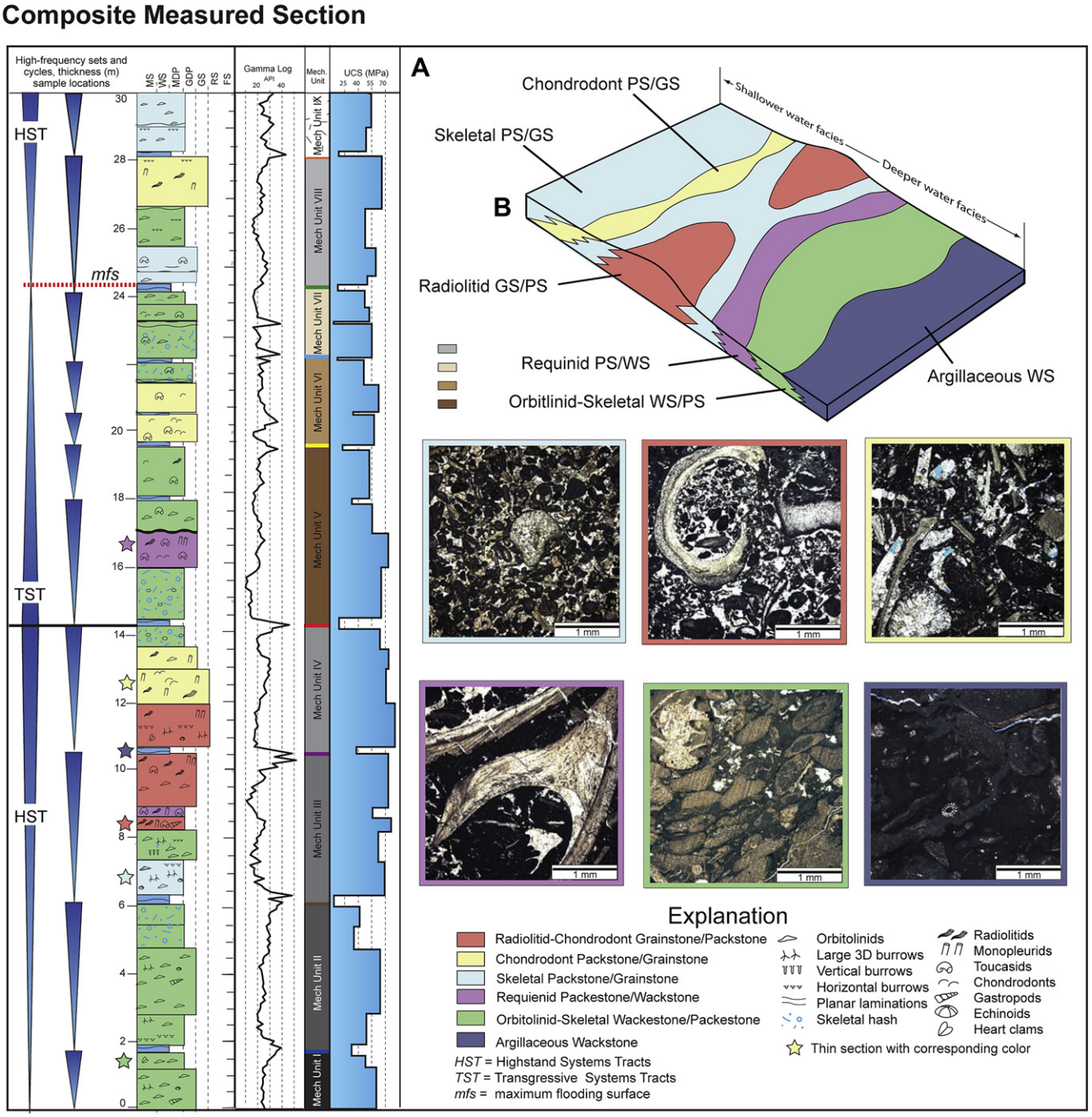

Fig. 3. Composite measured section for outcrop exposures, including high-frequency sets and cycles, thickness in meters, facies type, scintillometer gamma log, mechanical unit, and unconfined strength (MPa). Stars along measured section correspond to sampling locations for thin sections. (B) Schematic for deposition of facies present at this outcrop locality. Thin sections of each facies type have increasing carbonate mud content from upper left to lower right.

sections to determine the natural gamma ray response of the rocks, especially with the variable amounts of argillaceous material present in the section (Fig. 3). The gamma "log" also improves applicability as an analog outcrop for subsurface characterization. Fig. 3 is a summary of the measured section, including facies descriptions, example photomicrographs of each facies type, gamma log and a rock strength profile.

4. Outcrop characterization

This study characterizes two man-made exposures: (i) a road cut exposure (185 m long × 12 m high) along U.S. Highway 281 north of San Antonio, Texas, and (ii) a nearly adjoining and approximately perpendicular excavation wall (335 m long × 15 m high) as shown in Fig. 4. The road cut and excavation wall expose a local through going fault, here called the Main Fault, which has 5.1 m of offset and strikes northeast with a 55° dip to the southeast (Fig. 2). The excavation wall has an additional vertically continuous fault called the East Fault, which has 1.9 m of offset and is oriented 212° with a 64° dip to the northwest. Minor bedding dip changes occur locally near the faults, but most of the outcrop exposure has a bedding dip of 1–2° to the southeast. Numerous secondary faults (less than 1 m offset), shear fractures and opening-mode joints exposed in the outcrop were also mapped.

Detailed facies descriptions and discussion of the stratigraphic evolution of the section are beyond the scope of this paper, however a brief description of key facies is included and placed within a stratigraphic framework. The six facies identified in outcrop are: (1) radiolitid–chondrodont grain-dominated packstones to grainstones; (2) chondrodont wackestones to grain-dominated packstones; (3) mixed skeletal packstones to grainstones (4) requienid packstones; (5) orbitolinid-skeletal wackestones to packstones; and (6) argillaceous wackestones (Fig. 3). The facies are numbered by increasing depositional water depth, increasing mud content, and decreasing porosity and permeability. The radiolitid–chondrodont facies represents the highest-energy, shallowest water facies and the argillaceous wackestones represents the lowest-energy, relatively deepest water facies. These wackestones are also high in argillaceous clays, which indicate either an influx of terrigenous debris or much lower sedimentation rates allowing the higher percentage accumulation of insolubles relative to the carbonate sediments. Much of depositional environment of the facies interpreted in this portion of the outcrop can be described as shallow subtidal with a minimal amount of paleowater depth variation. The lateral continuity and vertical succession of these facies suggest an overall lower energy depositional environment in the interior platform setting.

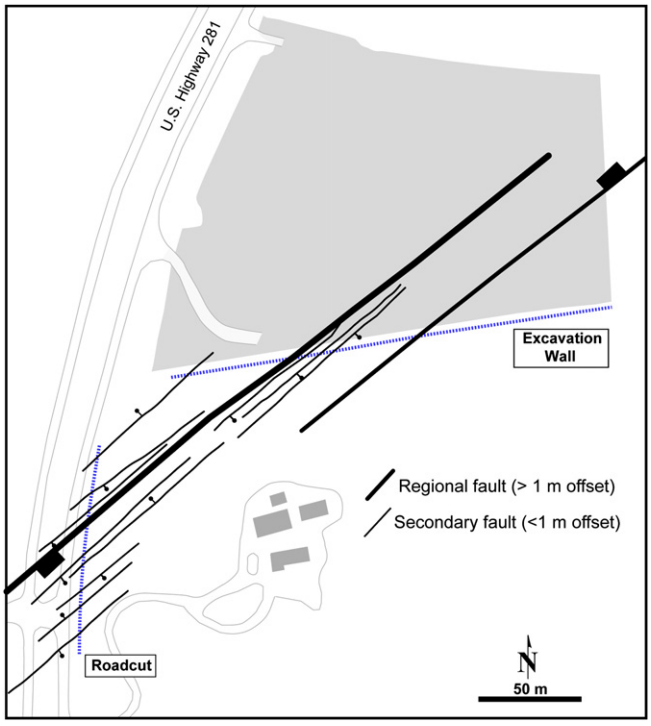

Fig. 4. Location of outcrops and mapped faults. Heavy lines are the main and East Faults whereas the lighter lines represent mapped secondary faults with less than 1 m of offset. Secondary fault traces are approximate, as their full extent cannot be determined from the outcrop trace.

The argillaceous wackestones represent a key marker in the stratigraphic succession. Their presence and frequency in a vertical succession are key observations to indicate that deposition occurred during a sea level rise event, thus comprising the transgressive systems tract (TST) of a high-frequency sequence. In contrast, where the argillaceous beds become further apart in a vertical succession paired with an increase in bed thickness and proportion of the more grain-rich facies (shown as the light blue, yellow, and red facies in Fig. 3) indicates an overall sea level fall event, or highstand systems tract (HST) of a high-frequency sequence. The pairing of the TST and HST comprises a single sea level rise and fall event. Each pair is bound by exposure events. As sea level rises, the platform is submerged in the TST and carbonate sedimentation is relatively low because the environmental conditions necessary have not developed leading to an accumulation of a higher proportion of fine-grained, clay material. After the maximum flooding of the platform, carbonate deposition and wave energy increase and relative sea level begins to fall. With increased wave energy significant winnowing of fine-grained material occurs and carbonate sedimentation rates are higher resulting in thicker, grainier facies in the HST (Gardner, 1995; Sonnenfeld and Cross, 1993). The stratigraphic position plays a critical role in the bed thickness and facies type which in turn impact the mechanical behavior of these units. Facies descriptions and thicknesses within the measured section were combined into composite stratigraphic cycles (Vail et al., 1977; Kerans and Fitchen, 1995) that vertically stack into a single sea level rise (transgressive systems tract or TST) and fall (highstand systems tract or HST) for the Albian 6 high-frequency sequence (Loucks and Kerans, 2003).

5. Deformation intensity characterization

The photopanoramic interpretation (Fig. 3) represents an integrated sampling of photo tracing, field checking and quantification by the lidar survey. Portions of the outcrop do not permit examination due to limited accessibility. The lidar survey was used to characterize the fracture intensity and orientation in these areas. For this outcrop, most fractures in the immediate vicinity of the larger faults or secondary faults are shear fractures, whereas the predominant fractures found in areas away from the faults (i.e., greater than 25 m distance) are opening-mode fractures. This is likely due to the processes associated with faulting, where the fault represents that linkage of opening-mode fractures into to shear fractures that eventually link to form either secondary or regional faults. We view the overall faulting process to be a continuum of deformation from opening-mode joints to faults.

We avoid the term fracture intensity characterization for the primary purpose that not all fractures could be field checked. For this reason, the term deformation intensity (DI) was chosen to represent the macroscopic, brittle deformation features present in the outcrop. Deformation intensity was characterized at both the excavation and road cut using a 0.5 × 0.5 m grid that was overlain

on top of the outcrop photo interpretation. Within each grid cell (2700 cells for the excavation exposure and 1534 from the road cut exposure), the entire trace length of all the fractures that crossed each grid cell were summed and divided by the grid area.

It has been shown that sampling bias may be introduced in outcrop exposures where fractures are not perpendicular to the outcrop face (Terzaghi, 1965). Fracture spacing or intensity measurements will not adequately reflect the true values if the exposed fractures are in apparent view. Most fractures exposed in this study are not perpendicular to the outcrop face. Therefore, the actual length of fracture trace was adjusted to correct for sample biasing of the outcrop orientation versus fracture orientation by multiplying the trace length by a fracture orientation weighting factor (W). This factor was determined for each individual fracture mapped on the outcrop photo trace and lidar survey as follows:

$$W = \sin(\delta)^{-1} \quad (1)$$

where δ is the acute angle between the outcrop face and the fracture of interest. As δ approaches 0°, the weighting factor becomes very large. Therefore, δ values less than 10° were artificially capped with a weighting value of four ($W = 4$). Less that 1% of all fractures measured in this study had δ values of less than 10°. Fractures oriented nearly parallel to the outcrop face receive the greatest degree of weighting compared to those that were perpendicular (Fig. 5).

Use of a length-weighted deformation intensity grid emphasizes the importance of secondary faults and the impact that they have on measured deformation (Fig. 6A). For this reason, the grid is a good map of the fault damage zones within this outcrop exposure. However, the influence of the stratigraphy on fracture development

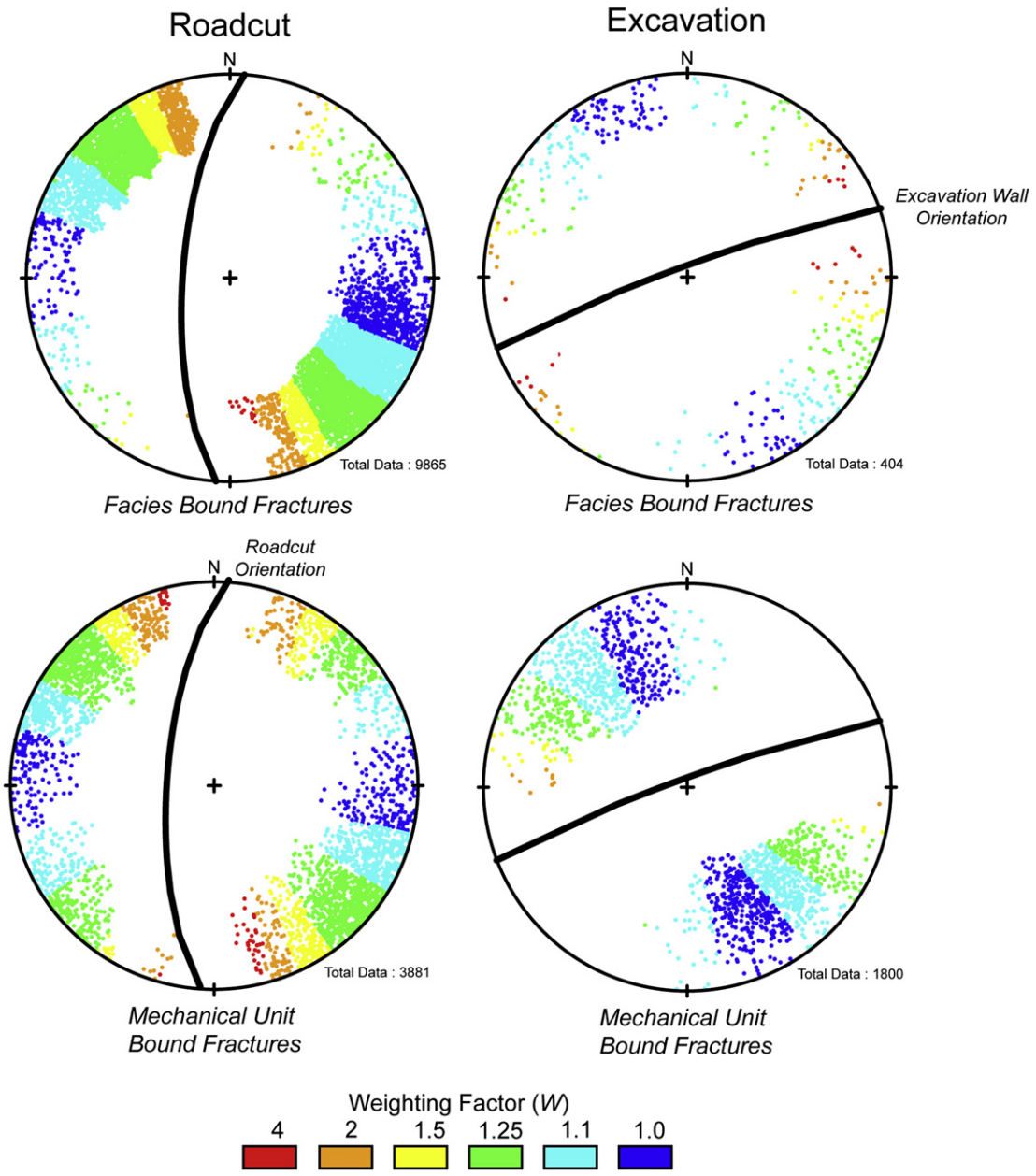

Fig. 5. Equal-area stereonets of lidar measured fracture orientations at the road cut and excavation outcrops. The upper equal-area net for each outcrop represents measured facies-bound fractures, whereas the lower stereonet represents mechanical-unit bound fractures. The great circle represents the average orientation of the outcrop face (both strike and dip). Fracture poles are colored by fracture orientation weighting factor (W).

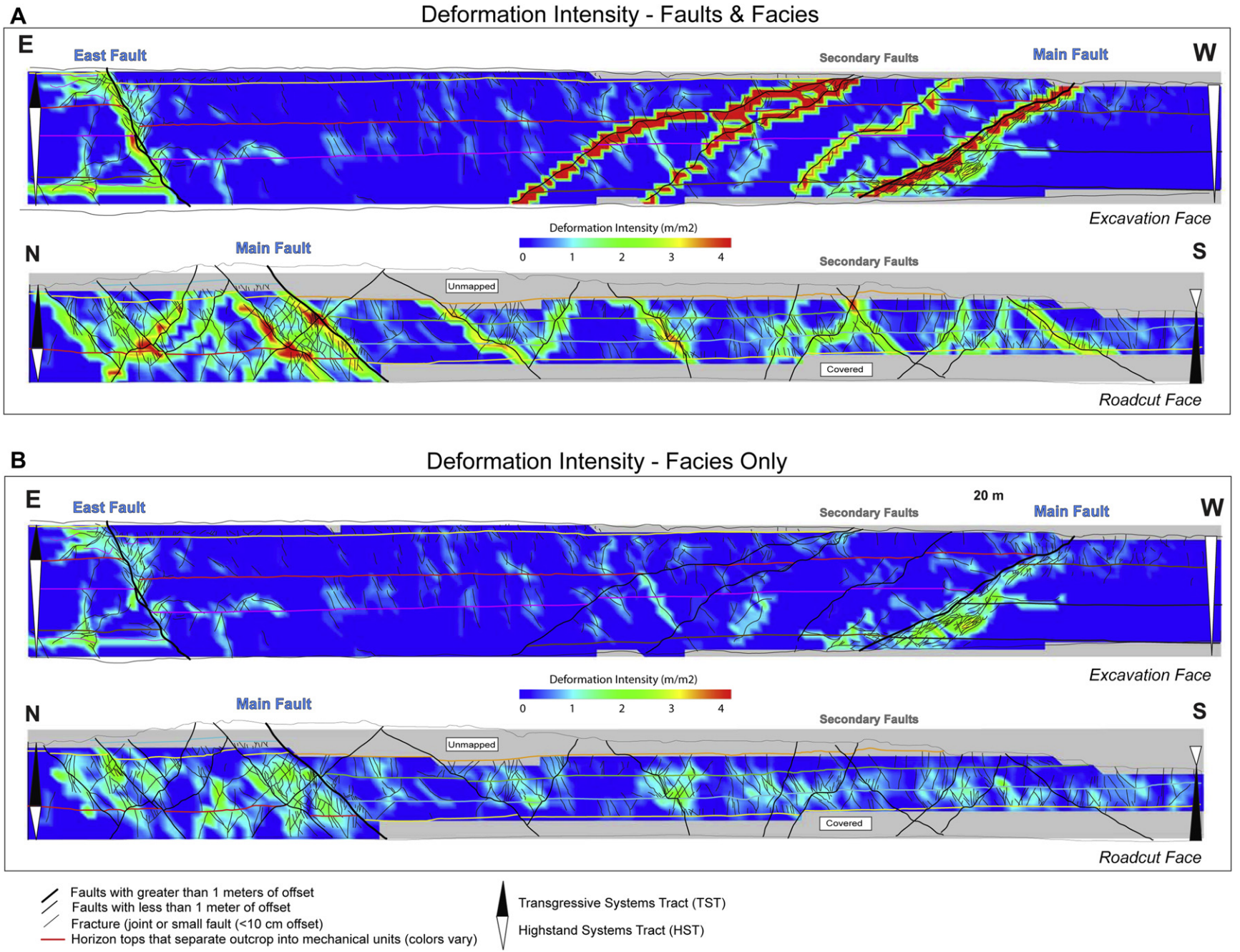

Fig. 6. Length-weighted deformation intensity grids of excavation and road cut outcrop exposures. The upper two grids represent the deformation when faults with greater than 0.1 m of offset where included. The lower two grids represent the deformation intensity when the faults were not included. Both grids have been corrected using the fracture orientation weighting factor.

is not well depicted in this figure. Therefore, the deformation intensity grid was recalculated without inclusion of the local or secondary fault traces (Fig. 6B). Within the same grids, mechanical units were mapped to provide a basis for comparison between the deformation intensity, mechanical units and stratigraphic systems tracts (Fig. 7).

6. Discussion

The deformation intensity represents an integrated measure of the dynamic interplay between the structural and stratigraphic framework, and aims to specifically address how the salient aspects of this deformation characterization relate to the stratigraphic cyclicity. This section will specifically address: (1) the rock strength characteristics of the nine mechanical units defined in this outcrop; (2) fracture terminations versus continuity for each of the mechanical units; (3) the impact of stratigraphy on fault style and characteristics; and (4) importance of fault damage zones in the context of stratigraphic cyclicity.

The composite measured section for this outcrop was divided into nine distinct mechanical units separated by nine recessive argillaceous wackestones that have a significantly lower calculated unconfined strength (14–20 MPa) when compared to the more resistant facies which averaged 54 MPa (range from 26 to 79 MPa). Fig. 3 illustrates UCS values for each of the facies within the composite measured section. A striking relationship is observed between the UCS values and the cyclicity of the facies. In the HST, the facies have very little mud, cycles are thicker, and rock strength is greater (mechanical units I–IV and VIII). The increase in rock strength corresponds to coarser grain sizes and higher grain-to-grain support along with an increase in the proportion of grains within the facies, which is greatest near the top of the HST cycle sets. In contrast, the TST cycle sets have a higher argillaceous component and cycles are thinner (mechanical units V–VII). The facies have a higher mud content and lower rock strength. The reduction in rock strength is further compounded by the thinner beds and increased vertical frequency of the argillaceous wackestone beds. While not a definitive argument, it does appear that the increase in carbonate mud content corresponds to lower rock strength (Fig. 3). The relative changes in rock strength as predicted by facies, in combination with bed or cycle thickness, dictate the type, geometry and style of fracture development.

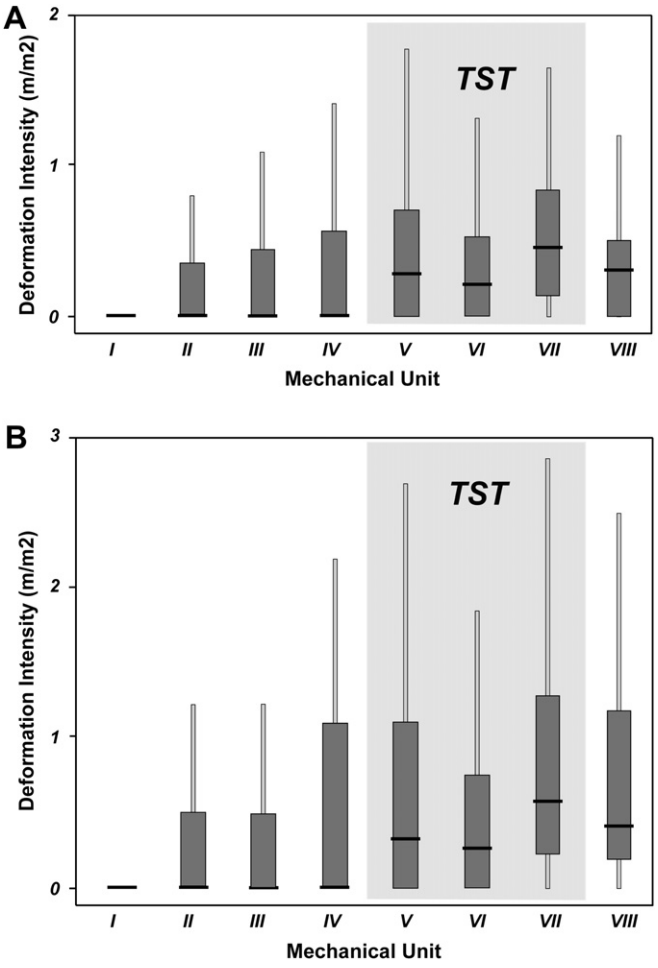

Fig. 7. Box-and-whisker plot of 2D deformation intensity (m/m^2) for each mechanical unit. Deformation is represented by quartiles (0, 25th, 50th, 75th and 97th) where the 50th quartile is the dark line, whereas the 25th and 75th are represented by the dark gray box and the 0 and 98th quartiles are show with thin light gray line. The transgressive systems tracts (TST) are shown within gray shaded region which is represented by mechanical units V–VII. (A) Plot for facies only without inclusion of the main and secondary faults. (B) Plot that includes facies and all faults in the calculation of deformation intensity.

Fractures occur at several scales at this outcrop locality. In general, there are three scales of interest—local faults with greater than 5 m of offset, secondary faults with 10 cm to 5 m of offset, and shear fractures and opening-mode joints that have little or no offset (Fig. 2). Within the fractures within no appreciable offset, the mechanical units have a significant influence on the vertical fracture terminations and the overriding control on fracture height is the presence of the laterally continuous argillaceous wackestones. Nearly 85% of the fracture heights terminate at the mechanical boundaries created by the nine argillaceous units found at the cycle boundaries. Approximately 5–10% of the vertical fracture terminations occur at the facies scale with fractures terminations at the bed boundary. The facies influence is higher in the TST cycles compared to the HST.

The correlation of the stratigraphic cyclicity on small fractures is apparent. Beyond this association, there is an additional link between secondary fault shape and cyclicity. The secondary faults in this outcrop exhibit numerous dip changes along their vertical trace. The greatest magnitude of change (e.g., from 70° to 10°) occurs at the contact between competent facies and the relatively incompetent argillaceous wackestone facies. At the excavation wall and road cut, significant fault dip change occurs between mechanical units IV and V, whereas secondary faults in the road cut have dip changes between mechanical units VI, VII and VIII (Fig. 2). Most of the significant dip changes in the secondary faults occur within the TST cycle sets. The mechanisms creating the fault dip change are discussed in detail by Ferrill and Morris (2003), but can generally be divided into two arguments. The first is through the linkage of vertical relays (Peacock and Zhang, 1994), whereby fractures propagate vertically from the brittle, higher strength units into units of lower strength. As extension continues, the brittle fractures are linked along a system of vertical relays. Conversely, Ferrill and Morris (2003) suggest a mechanism by which the variability of rock strength in conjunction with low values of effective stress and a minimum principal effective stress cause different layers to deformation by dilatational normal faulting, thereby generating different fracture orientations from bed to bed. In both arguments, it is the thinner cycle sets, which are common to the TST, that provides the framework for complex secondary fault geometry. Fault development occurs during deformation at a low value of minimum principal stress, but the secondary fault dip through the mechanically weak horizons is 10–15°, which is an extremely low angle for dilatational failure, even for mechanically weak horizons. This suggests that the faults linkages are more likely

Table 1
Summary of deformation intensity (m/m^2) by systems tract and mechanical unit illustrated in Fig. 7. For each mechanical unit, the 25th, 50th, 75th, and 97th quartiles are given along with the mean deformation intensity. The values are provided for both the facies only and facies plus fault case.

Mechanical unit		Type	25th quartile	50th quartile	75th quartile	97th quartile	Mean
HST	VIII	Facies only	0	0.31	0.51	1.3	0.36
		Fault and facies	0.19	0.41	1.2	4.3	0.98
TST	VII	Facies only	0.14	0.46	0.84	1.7	0.55
		Fault and facies	0.22	0.57	1.3	4.3	1.1
	VI	Facies only	0	0.21	0.53	1.3	0.34
		Fault and facies	0	0.27	0.75	3.8	0.74
	V	Facies only	0	0.29	0.71	1.8	0.45
		Fault and facies	0	0.33	1.1	7.3	1.1
HST	VI	Facies only	0	0	0.57	1.6	0.34
		Fault and facies	0	0	0.9	9.5	1.1
	III	Facies only	0	0	0.44	1.8	0.27
		Fault and facies	0	0	0.5	6.6	0.63
	II	Facies only	0	0	0.35	2.5	0.37
		Fault and facies	0	0	0.5	7	0.84
	I	Facies only	0	0	0	3.7	0.49
		Fault and facies	0	0	0	8.1	0.74

the result of vertical relay development rather than pure mechanical dilatation.

Change in secondary fault dip has an additional consequence in the context of fracture development. Each refraction point along the secondary faults creates an asperity in the fault that complicates further slip along the fault, similar to contractional bends in Peacock and Zhang (1994). The asperity points cause additional fractures in the hanging wall, and to a lesser extent footwall, leading to increased deformation (Fig. 6). This mechanism contributes significantly to the higher deformation intensity within the TST compared to HST in Figs. 6B and 7. The data suggests that the degree of deformation attributed to the dip change in the secondary faults is controlled by the relative thickness of the argillaceous units. If the argillaceous unit were thick, the asperity would be larger and therefore the deformation intensity would be higher in the vicinity of the asperity. This is observed in secondary faults along the road cut exposure, shown in Fig. 6B. In this case, the argillaceous wackestone that separates mechanical units IV and V is thick, creating a large asperity and all the secondary faults within the hanging wall of the Main Fault. At this scale, it can be observed that the variability in stratigraphy has created a large fault damage zone for a relatively small fault offset (e.g., compared to Peacock and Sanderson, 1994; Shultz and Fossen, 2002).

Deformation intensity within the fault damage zones of both the secondary and regional faults have a variable response based on the stratigraphic facies and systems tracts that the faults are cross-cutting (Fig. 6). Deformation intensity in mechanical unit V along the road cut exposure is an excellent example of increased fracture development within secondary fault damage zones (Figs. 3 and 6). Contrast the deformation of mechanical unit V to the style of deformation observed in mechanical units III and IV in the excavation exposure, where very little additional fracturing developed along the secondary faults. The importance of considering deformation within the stratigraphic architecture is best quantitatively analyzed. Box-and-whisker plots of the deformation intensity within each mechanical unit highlight the increased amount of deformation in the TST versus HST (Fig. 7 and Table 1). Mechanical unit VIII, part of the overlying HST, has increased values of deformation intensity, which we attribute to the high concentration of secondary faults with unusual geometries (e.g., stair-stepping profile) in the underlying TST. While the faulting does cause an overall increase in deformation intensity values (Fig. 7B and Table 1), the facies and stratigraphic architecture still control the primary response as evident by the similar deformation intensity profile illustrated in Fig. 7A and B. The results of this characterization highlight the importance of stratigraphy in the deformation process. The interplay between the fault zone dynamics and the stratigraphic integrity must be incorporated equally to accurately characterize the geologic system.

7. Conclusions

Deformation in layered, inherently anisotropic rocks is variable in the style, location and extent of fracture development, making predictions difficult. This paper characterizes fracture development within an extensional fault zone using a systematic sequence stratigraphic framework, thereby providing a context for improved predictability of fracture development in the subsurface and that can be easily integrated with facies-based models of matrix properties. The characterization of carbonate facies in this study has illustrated that significant rock strength variability can occur even in a vertical succession of 30 m and the facies heterogeneity influences the overall deformation and fault development geometry. The predictability of fractures by systems tracts can be used to guide the style and scale of fractures that may develop in the interwell regions in the subsurface. We have shown that within the highstand systems tract facies are thicker, more grain-dominated and more competent. Facies within the transgressive systems tracts are thinner, less grain-dominated, and less competent. The implications are that deformation intensity in the HST is lower than the TST owing to a combination of mud content, cycle thickness, rock strength and additional fracture development related to asperities in secondary faults caused by the rock strength variability.

Based on this study, an *a priori* prediction of fracture permeability may be possible using a characterized sequence stratigraphic architecture. Fracture size is strongly dependent on bed thickness and fractures contained within thinner mechanical units are limited in length, aperture, and connectivity compared to fractures within thicker beds (Shultz and Fossen, 2002). Other researchers have reported a correlation between fracture apertures being larger in longer fractures (Pollard and Segall, 1987; Renshaw and Park, 1997; Bai et al., 2000; Olson, 2003). Furthermore, fracture

connectivity has a lower percolation threshold (i.e., more connected) if fractures are longer and taller (Odling, 1997; De Dreuzy et al., 2001; Manzocchi, 2002). These observations suggest that the most significant fractures with respect to permeability are the tallest or longest fractures within the system of interest. Furthermore, systematic prediction of the significant fractures is critical for developing models of dual permeability systems. Integrated reservoir models of facies distribution are common, but correlation between these facies and the fracture distribution provides an elegant methodology for distributing fractures within subsurface models. An integrated facies and fracture model allows for calibration to hydraulic conditions in both static and dynamic reservoir models.

Fractures that are significant to permeability enhancement or anisotropic flow may be more commonly found in the HST, where the taller, longer and more connected fractures are more likely to develop compared to the TST. Although the TST may have higher fracture intensity than the HST, the HST has a greater impact on permeability as a result of size of the developed fractures. We contend that characterization of carbonate fault damage zones in absence of a stratigraphic framework will always give a misleading prediction of fracture distribution and, ultimately, permeability within the fractured subsurface.

Acknowledgements

The authors would like to thank the H.L. Chapman Pipeline Company for access to the excavation exposure and for ability to collect samples for analysis. This work was originally supported by the Subsurface Technology Group of ConocoPhillips. Subsequent work has been supported by members of the Reservoir Characterization Research Laboratory (RCRL) industrial associates program at the Bureau of Economic Geology at the University of Texas at Austin. Thorough review of the original manuscript by David Ferrill, Fabrizio Agosta and an additional reviewer greatly improved the content and clarity of this manuscript. Additional improvements have been made through valuable discussions with Charles Kerans, Alan Morris, Bob Krantz, Peter Hennings, and Xavier Janson. Publications costs were supported foundation of the Jackson School of Geosciences. This work is published with consent of the Dr. Scott Tinker, Director of the Bureau of Economic Geology.

References

Bai, T., Pollard, D.D., 2000. Fracture spacing in layered rocks: a new explanation. Journal of Structural Geology 22, 43–57.

Bai, T., Pollard, D.D., Gross, M.R., 2000. Mechanical prediction of fracture aperture in layered rocks. Journal of Geophysical Research 105, 707–721.

Biot, M.A., Medlin, W.L., Masse, L., 1983. Fracture penetration through an interface. Society of Petroleum Engineers Journal 23, 857–869.

Caine, J.S., Evans, J.P., Forster, C.B., 1996. Fault zone architecture and permeability structure. Geology 24, 1025–1028.

Childs, C., Nicol, A., Walsh, J.J., Watterson, J., 1996. Growth of vertically segmented normal faults. Journal of Structural Geology 18, 1389–1397.

Collins, E.W., Hovorka, S.D., 1997. Structure Map of the San Antonio Segment of the Edwards Aquifer and Balcones Fault Zone, South-central Texas: Structural Framework of a Major Limestone Aquifer. University of Texas, Kinney, Uvalde, Medina, Bexar, Comal, and Hays Counties, Austin. Bureau of Economic Geology Miscellaneous Map 38, scale 1:250,000, 2 sheets.

Collins, E.W., 2000. Geologic Map of the New Braunfels, Texas, 30 × 60 Minute Quadrangle: Geologic Framework of an Urban-growth Corridor Along the Edwards Aquifer, South-central Texas. University of Texas. Bureau of Economic Geology Miscellaneous Map 39, scale 1: 100,000, 1 sheet.

Cook, T.S., Erdogan, F., 1972. Stresses in bonded materials with a crack perpendicular to the interface. International Journal of Engineering Science 10, 677–697.

Corbett, K., Friedman, M., Spang, J., 1987. Fracture development and mechanical stratigraphy of Austin Chalk, Texas. The American Association of Petroleum Geologists Bulletin 71, 17–28.

Cox, S.J.D., Scholz, C.H., 1988. On the formation and growth of faults: an experimental study. Journal of Structural Geology 10, 413–430.

Deere, D.U., Miller, R.P., 1966. Engineering Classification and Index Properties for Intact Rock. Report AFWL-TR-65-116. Air Force Systems Command, Kirtland Air Force Base, New Mexico.

De Dreuzy, J.R., Davy, P., Bour, O., 2001. Hydraulic properties of two-dimensional random fracture networks following a power law length distribution 2. Permeability of networks based on lognormal distribution of apertures. Water Resources Research 37 (8), 2079–2095.

Dunham, R.J., 1962. Classification of carbonate rocks according to depositional texture. In: Ham, W.E. (Ed.), Classification of Carbonate Rocks. American Association of Petroleum Geologists Memoir 1, pp. 108–121.

Ferrill, D.A., Morris, A.P., 2003. Dilational normal faults. Journal of Structural Geology 25, 183–196.

Ferrill, D.A., Morris, A.P., 2008. Fault zone deformation controlled by carbonate mechanical stratigraphy, Balcones fault system, Texas. American Association of Petroleum Geologists Bulletin 92 (3), 359–380.

Friedman, M., Kwon, O., French, V.L., 1994. Containment of natural fractures in brittle beds of the Austin Chalk, rock mechanics, models and measurements challenges from industry. In: Nelson, P.P., Laubach, S.E. (Eds.), Proceedings of the First North American Rock Mechanics Symposium. Balkema, Texas, Austin, pp. 833–840.

Gardner, M.H., August 1995. Accommodation controls on fluvial-deltaic reservoir architecture. AAPG Bulletin 79 (8), 1213.

Goldhammer, R.K., 1999. In: Bartolini, C., Wilson, J.L., Lawton, T.F. (Eds.), Mesozoic Sedimentary and Tectonic History of North-Central Mexico. Geological Society of America, Special Paper , vol. 340, 380 pp.

Gross, M.R., Eyal, Y., 2007. Throughgoing fractures in layered carbonate rocks. Geological Society of America Bulletin 119 (11-12), 1387–1404.

Gross, M.R., 1993. The origin and spacing of cross joints: example from the Monterey Formation, Santa Barbara Coastline, California. Journal of Structural Geology 15, 737–751.

Gross, M.R., Fischer, M.P., Engelder, T., Greenfield, R.J., 1995. Factors controlling joint spacing in interbedded sedimentary rocks: interpreting numerical models with field observations from the Monterey Formation, USA. In: Ameen, M.S. (Ed.), Fractography: Fracture Topography as a Tool in Fracture Mechanics and Stress Analysis. Geological Society of America, Special Publication, vol. 93, pp. 215–233.

Hill, R.T., January 1890. Classification and origin of the chief geographic features of the Texas region. The American Geologist 6, 9–29.

Huang, Q., Angelier, J., 1989. Fracture spacing and its relation to bed thickness. Geological Magazine 126, 355–362.

Huang, Y., Zhang, H.W., 1995. The role of metal plasticity and interfacial strength in the cracking of metal/ceramic laminates. Acta Metallurgica et Materialia 43, 1523–1530.

Hovorka, S.D., Mace, R.E., Collins, E.W., 1998. Permeability Structure of the Edwards Aquifer, South Texas—Implications for Aquifer Management. Bureau of Economic Geology, University of Texas at Austin, Austin, Texas, Report of Investigations 250, 55 pp.

Janson, X., Kerans, C., Bellian, J.A., Fitchen, W., 2007. Three-dimensional geological and synthetic seismic model of Early Permian redeposited basinal carbonate deposits, Victorio Canyon, west Texas. AAPG Bulletin 91, 1405–1436.

Kerans, C., Fitchen, W.M., 1995. Sequence Hierarchy and Facies Architecture of a Carbonate-Ramp System: San Andres Formation of Algerita Escarpment and Western Guadalupe Mountains, West Texas and New Mexico. The University of Texas at Austin, Bureau of Economic Geology. Report of Investigations No. 235, 86 pages with plates.

Kerans, C.K., Loucks, R.G., 2002. Stratigraphic setting and controls on occurrence of high-energy carbonate beach deposits: lower cretaceous of the Gulf of Mexico. Gulf Coast Association of Geological Societies Transactions 52, 517–526.

Ladeira, F.L., Price, N.J., 1981. Relationship between fracture spacing and bed thickness. Journal of Structural Geology 3, 179–183.

Lorenz, J.C., Sterling, J.L., Schechter, D.S., Whigham, C.L., Jensen, J.J., 2002. Natural fractures in the Sprayberry Formation, Midland Basin, Texas: the effects of mechanical stratigraphy on fracture variability and reservoir behavior. American Association of Petroleum Geologists Bulletin 86, 505–524.

Loucks, R.L., Kerans, C., 2003. Lower cretaceous Glen Rose "Patch Reef" reservoir in the Chittim field, Maverick County, South Texas. Gulf Coast Association of Geological Societies Transactions 53, 490–503.

Lucia, F.J., 1995. Rock-fabric/petrophysical classification of carbonate pore space for reservoir characterization. AAPG Bulletin 79 (9), 1275–1300.

Manzocchi, T., 2002. The connectivity of two-dimensional networks of spatially correlated fractures. Water Resources Research 38 (9), 1162–1182.

McQuillan, H., 1973. Small-scale fracture density in Asmari formation of Southwest Iran and its relation to bed thickness and structural setting. American Association of Petroleum Geologists Bulletin 57, 2367–2385.

Narr, W., Suppe, J., 1991. Joint spacing in sedimentary rocks. Journal of Structural Geology 13, 1037–1048.

Odling, N., 1997. Scaling and connectivity of joint systems in sandstones from western Norway. Journal of Structural Geology 19 (10), 1257–1271.

Olson, J.E., 2003. Sublinear scaling of fracture aperture versus length: an exception or the rule? Journal of Geophysical Research 108 (B9), 2413–2414.

Peacock, D.C.P., Sanderson, D.J., 1994. Geometry and development of relay ramps in normal fault systems. American Association of Petroleum Geologists Bulletin 78 (2), 147–165.

Peacock, D.C.P., Zhang, X., 1994. Field examples of numerical modeling oversteps and bends along normal faults in cross section. Tectonophysics 234, 147–167.

Pollard, D.D., Segall, P., 1987. Theoretical displacements and stresses near fractures in rock: with applications to faults, joints, veins, dikes and solution surfaces. In: Atkinson, B.K. (Ed.), Fracture Mechanics of Rock. Academic, San Diego, Calif, pp. 277–350.

Poole, R.W., Farmer, I.W., 1980. Consistency and repeatability of Schmidt Hammer rebound data during field testing. International Journal of Rock Mechanics and Mining Science & Geomechanics Abstracts 17, 167–171.

Read, J.F., 1995. Overview of carbonate platform sequences, cycle stratigraphy and reservoirs in greenhouse and ice-house worlds. In: Read, J.F., Kerans, C., Weber, L.J., Sarg, J.F., Wright, F.M. (Eds.), Milankovitch Sea-level Changes, Cycles and Reservoirs on Carbonate Platforms in Greenhouse and Ice-house Worlds SEPM Short Course Notes 35.

Renshaw, C.E., Park, J.C., 1997. Effect of mechanical interactions on the scaling of fracture length and aperture. Nature 386, 482–484.

Renshaw, C.E., Myse, T.A., Brown, S.R., 2003. Role of heterogeneity in elastic properties and layer thickness in the jointing of layered sedimentary rocks. Geophysical Research Letters 24, 2295.

Rijken, P., Cooke, M.L., 2001. Role of shale thickness on vertical connectivity of fractures: application of crack-bridging theory to the Austin Chalk, Texas. Tectonophysics 337 (1–2), 117–133.

Shultz, R.A., Fossen, H., 2002. Displacement–length scaling in three dimensions: the importance of aspect ratio and application to deformation bands. Journal of Structural Geology 24, 1389–1411.

Schopfer, M.J.P., Childs, C., Walsh, J.J., Manzocchi, T., Koyi, H.A., 2007. Geometrical analysis of the refraction and segmentation of normal faults in periodically layered sequences. Journal of Structural Geology 29, 318–335.

Sellards, E.H., 1919. The geology and mineral resources of Bexar County. University of Texas Bulletin 1932, 7–97.

Sonnenfeld, M., Cross, T., 1993. Volumetric partitioning and facies differentiation within the Permian upper San Andres Formation of Last Chance Canyon, Guadalupe Mountains, New Mexico. In: Loucks, Robert, G., Sarg, J., Frederick (Eds.), Carbonate Sequence Stratigraphy; Recent Developments and Applications. American Association of Petroleum Geologists Memoir 57, pp. 435–474.

Terzaghi, R.D., 1965. Sources of error in joint surveys. Geotechnique 15, 287–304.

Thiercelin, M., Roegiers, J.C., Boone, T.J., Ingraffea, A.R., 1987. An investigation of the material parameters that govern the behavior of fractures approaching rock interfaces. In: Proceedings of the Sixth International Congress on Rock Mechanics, pp. 263–269.

Treagus, S.H., 1988. Strain refraction in layered systems. Journal of Structural Geology 10, 517–527.

Underwood, C.A., Cooke, M.L., Simo, J.A., Muldoon, M.A., 2003. Stratigraphic controls on vertical fracture patterns in Silurian dolomite, northeastern Wisconsin. AAPG Bulletin 87 (1), 121–142.

Vail, P.R., Mitchum Jr., R.M., Todd, R.G., Widmier, J.M., Thompson III, S., Sangree, J.B., Bubb, J.N., 1977. Seismic stratigraphy and global changes of sea level. In: Payton, C.E. (Ed.), Seismic stratigraphy-applications to hydrocarbon exploration. American Association of Petroleum Geologists Memoir 26, pp. 49–205.

Walsh, J.J., Bailey, W.R., Childs, C., Nicol, A., Bonson, C.G., 2003. Formation of segmented normal faults: a 3-D perspective. Journal of Structural Geology 25, 1251–1262.

Walsh, J.J., Watterson, J., Bailey, W.R., Childs, C., 1999. Fault relays, bends and branch-lines. Journal of Structural Geology 21, 1019–1026.

Weeks, A.W., 1945. Balcones, Luling, and Mexica fault zones in Texas. American Association of Petroleum Geologists Bulletin 29, 1733–1737.

Wilkins, S.J., Gross, M.R., 2001. Normal fault growth in layered rocks at Split Mountain, Utah: influence of mechanical stratigraphy on dip linkage, fault restriction and fault scaling. Journal of Structural Geology 24, 1413–1429.

Wu, H., Pollard, D.D., 1995. An experimental study of the relationship between joint spacing and layer thickness. Journal of Structural Geology 17, 887–905.